catalysts

MDPI

Article

Shining a Light on Sewage Treatment: Building a High-Activity and Long-Lasting Photocatalytic Reactor with the Elegance of a "Kongming Lantern"

Xiaohan Xu [1,2], Yi Wang [1,2,*], Zhuo Deng [1,2], Jin Wang [1], Xile Wei [1], Peng Wang [1,2] and Dun Zhang [1,2]

[1] Key Laboratory of Advanced Marine Materials, Key Laboratory of Marine Environmental Corrosion and Bio-Fouling, Institute of Oceanology, Chinese Academy of Sciences, Qingdao 266071, China; xuxiaohan@qdio.ac.cn (X.X.); dengzhuo5015@163.com (Z.D.); wangjin@qdio.ac.cn (J.W.); 15836956680@163.com (X.W.); wangpeng@qdio.ac.cn (P.W.); zhangdun@qdio.ac.cn (D.Z.)

[2] University of the Chinese Academy of Sciences, 19 (Jia) Yuquan Road, Beijing 100039, China

* Correspondence: wangyi@qdio.ac.cn; Tel.: +86-532-82893612

Abstract: Photocatalysis is a promising technology for efficient sewage treatment, and designing a reactor with a stable loading technique is crucial for achieving long-term stability. However, there is a need to improve the current state of the art in both reactor design and loading techniques to ensure reliable and efficient performance. In this study, we propose an innovative solution by employing polydimethylsiloxane as a bonding layer on a substrate of 3D-printed polyacrylic resin. By means of mechanical extrusion, the active layer interacts with the bonding layer, ensuring a stable loading of the active layer onto the substrate. Simultaneously, 3D printing technology is utilized to construct a photocatalytic reactor resembling a "Kongming Lantern", guaranteeing both high activity and durability. The reactor exhibited remarkable performance in degrading organic dyes and eliminating microbes and displayed a satisfactory purification effect on real water samples. Most significantly, it maintained its catalytic activity even after 50 weeks of cyclic degradation. This study contributes to the development of improved photocatalysis technologies for long-term sewage treatment applications.

Keywords: photocatalysis; reactor; loading technique; long-term life; sewage treatment

Citation: Xu, X.; Wang, Y.; Deng, Z.; Wang, J.; Wei, X.; Wang, P.; Zhang, D. Shining a Light on Sewage Treatment: Building a High-Activity and Long-Lasting Photocatalytic Reactor with the Elegance of a "Kongming Lantern". *Catalysts* **2024**, *14*, 645. https://doi.org/10.3390/catal14090645

Academic Editors: Eduardo Miró, Ezequiel David Banus and Juan Pablo Bortolozzi

Received: 27 August 2024
Revised: 15 September 2024
Accepted: 18 September 2024
Published: 21 September 2024

1. Introduction

In recent years, the rapid development of the social economy and urbanization has led to an increasing demand for water resources in every country [1,2]. However, this has resulted in a significant rise in water pollution, which poses new challenges to conventional sewage treatment technologies [3]. Therefore, it is imperative to develop green, environmentally friendly, and efficient sewage treatment technologies in order to achieve the goal of "double carbon", encompassing both carbon peak and carbon neutrality [4,5]. Hence, there is an urgent need to address these challenges and develop responsive sewage treatment technologies that are sustainable, eco-friendly, and efficient.

Advanced oxidation technology (AOP) involves the generation of highly reactive oxygen species (ROS) with strong oxidation capabilities, accomplished through various means such as a high temperature, pressure, light, electricity, and sound [6]. These ROS possess the ability to oxidize complex organic compounds that are difficult to degrade in water, converting them into smaller, less toxic molecules. Common AOP methods comprise photochemical oxidation, acoustic chemical oxidation, ozone oxidation, electrochemical oxidation, and Fenton oxidation. Among these methods, photocatalytic oxidation stands out as a technology that aligns best with the requirements of environmentally friendly carbon sinks [7]. It utilizes semiconductor materials with specific energy band structures to treat slightly polluted water environments by degrading or eliminating both organic pollutants

and harmful microorganisms. Despite continuous research efforts, the development of various photocatalyst materials with broad-spectrum responses in line with the principles of green development has been achieved. Examples of such materials include bismuth-based materials [8], tungsten-based materials [9], and g-C_3N_4 [10]. However, nanoparticle photocatalyst materials encounter the drawback of being challenging to recover and reuse once introduced into water [7]. Therefore, the implementation of catalyst supports is an effective approach to enable the recycling of photocatalysts and prevent them from causing secondary pollution in water [11–15].

Currently, the commonly used support methods for photocatalysts include the in situ growth method [16–19] and the spraying method [20–22]. Previously, Xu et al. [18] prepared Ag-modified β-Bi_2O_3/$Bi_2O_{2.7}$ heterostructure films on a polyvinyl chloride (PVC) polymer matrix using the one-step hydrothermal method, which showed that the degradation rate of Rhodamine B (Rh B) reached 97% within 150 min. The inactivation rate of *Escherichia coli* (*E. coli*) was >99.99% within 18 h, and it had anti-adhesion properties of *Escherichia coli*. Meanwhile, Liu et al. [23] prepared a photocatalytic coating based on WO_3-TiO_2 nanorods (MWT)/PDMS on the substrate using the spraying method. The superhydrophobic properties of the surface give it the function of self-cleaning and allow it to degrade surface organic pollutants. However, after five cycles of degradation, the degradation efficiency of NO under visible light gradually decreased by 4.74% without special treatment due to the adhesion of oxidation products. A comparison of the two methods revealed that the spraying method allows for a strong attachment of the photocatalytic material to the substrate. However, the presence of the coating hinders the exposure of certain active sites. In contrast, the in situ growth method demonstrates higher activity and a faster degradation rate. Nevertheless, the film tends to detach over time in real water conditions due to the weak bond between the film layer and the substrate. As a result, this reduces durability, leading to potential secondary pollution in the water environment. Hence, it is crucial to identify a method that achieves a balance between activity and longevity, specifically by providing an appropriate binding force at the interface [24].

The utilization of polymeric materials, including polyacrylonitrile, polyvinylidene fluoride, polystyrene, polymethyl methacrylate, waterborne polyurethane, and polyethylene terephthalate, has recently emerged as a viable solution for fabricating photocatalytic films [25–30]. In photocatalytic reactors, polydimethylsiloxane (PDMS) is commonly employed due to its exceptional properties such as high optical transparency, heat resistance, and chemical inertness [31–33]. However, methods like electrospinning, direct spraying, or dipping onto metal sheet/mesh, conductive glass, or polymer fiber substrates often result in weak adhesion between the photocatalytic active layer and the substrate [34]. Li et al. [35] used electrodeposition technology to prepare a two-dimensional g-C_3N_4/Cu_2O/Cu composite coating on a 316L stainless steel surface. Due to the synergistic bactericidal effect of copper ions and the production of reactive oxygen species promoted by the coating, the coating quickly eliminated *Escherichia coli* and *Staphylococcus aureus* within 1 h under both light and dark conditions. Therefore, achieving a firm and uniform active layer on the substrate is crucial. In this study, we propose a novel approach using a mechanical extrusion method to prepare photocatalytic reactor components with three layers: a substrate, binder layer, and active layer.

Three-dimensional printing, an additive manufacturing technology that has undergone decades of development and maturation [36], converts 3D model data into intricate objects by adding materials. This straightforward and efficient technology has the potential to create optimized substrate structures for photocatalysts, including complex designs [37–39], resulting in an enhanced specific surface area and an increased load capacity of the photocatalytic material. Moreover, widely used polymer materials such as polypropylene resin and epoxy resin [40–43] not only enable the production of transparent substrates, improving the efficiency of light transmission during the reaction process, but also fulfill the requirements of green chemistry due to their odorless and non-toxic properties. Furthermore, substrates manufactured through 3D printing exhibit remarkable mechanical and

chemical stability, making them affordable and allowing for rapid production. In previous studies, 3D printing has been combined with photocatalyst loads to build photocatalytic reactors that can be used for water purification. In the study by Zheng et al. [38], they fixed photocatalyzed graphite carbon nitride onto chitosan to prepare g-C_3N_4/chitosan hydrogel beads (GCHB) and filled them in quartz tubes, and then they used 3D printing technology to fabricate reflectors for CPC reactors and used them to adhere reflected aluminum bands. Schreck et al. [44] proposed an aerogel that used a 3D-printed polymer scaffold to support nanoparticles and optimized its photocatalytic performance by adjusting the geometry of the scaffold to control the geometry of the photocatalyst for the photocatalytic reaction. Xu et al. [45] proposed a simple method for synthesizing iodine-deficient BiOI-engineered films on 3D-printed polymers at mild room temperature and pressure by adjusting the pH of the BiOI solution only. Although the degradation rate of Rh B was 99.67% and the inactivation rate of Escherichia coli was >99.99%, the photocatalytic performance decreased significantly, and the surface film fell off with the progress of cyclic sterilization degradation times. Hence, they are favorable choices for constructing photocatalytic reactors and treating polluted water environments [46,47].

The objective of this study is to employ PDMS as a binder to fabricate a durable and efficient photocatalytic water purification device, resembling a "Kongming Lantern", by creating a photocatalytic active layer on a 3D-printed substrate in an environmentally friendly manner. Instances of photocatalytic water purification devices demonstrating both stable, effective catalytic activity, and longevity are limited, making this work highly distinctive and innovative. Firstly, a scanning electron microscope (SEM, Regulus 8100, Hitachi, Ibaraki, Japan) was used to examine the surface of the active layer and its adhesive interaction with the binding layer. Subsequently, the photocatalytic activity of the reactor was evaluated using common model dyes and bacteria, including Rhodamine B (Rh B), methylene blue (MB), *Escherichia coli* (*E. coli*), and *Staphylococcus aureus* (*S. aureus*), and the effectiveness was determined through testing with actual water samples. Finally, cyclic experiments and simulated scour experiments were conducted to verify the load stability of the photocatalytic active layer. This strategy enhances the current state of the art in reactor design and loading techniques, aiming to ensure reliable and efficient performance.

2. Results

2.1. The Characterization of the Reactor

Figure 1a illustrates the optical changes observed on the substrate's surface during the preparation of the photocatalytic active layer. In Figure 1a, (i) shows the original substrate, (ii) shows the substrate brushed with PDMS resin, (iii) shows the PDMS layer shaken with BiOI powder, and (iv) shows the substrate after mechanical extrusion. Figure 1c reveals that the mechanical extrusion used in layer preparation results in an uneven distribution of BiOI powder in the groove and varying thicknesses of the PDMS brush on the bonding layer, leading to an uneven surface thickness. Figure 1d,f,g further demonstrate that in certain areas, PDMS flows into the gaps between materials and wraps around BiOI. This occurrence is a result of the interaction between the adhesive layer and the surface's active layer, wherein the extrusion force exerted by the vice pushes the BiOI material into the adhesive layer, simultaneously causing the PDMS to wrap the catalyst material on the surface. Consequently, BiOI becomes firmly fixed on the surface, forming a photocatalytic active layer due to its adhesive properties. This observation is confirmed by Figure 1h, which showcases some BiOI particles in the adhesive layer as a result of the mutual extrusion force between layers. Additionally, specific regions like that shown in Figure 1e display an exposed adhesive layer or substrate, possibly due to inadequate compaction of the powder in the groove and insufficient PDMS content to hold the catalyst material in place. It is worth noting that for a photocatalytic active layer, the exposure of active sites to reactants is crucial. Considering that PDMS spills into the material due to mechanical extrusion, the element distribution on the active layer surface is characterized using EDS (Bruker xflash3160 spectrometer, Billerica, MA, USA). Figure 2 demonstrates the evenly

distributed and abundant catalyst components Bi and I in the randomly selected region, while the main components of PDMS (C, O, and Si) are equally distributed in this area. This verifies that the active sites are exposed on the surface, promoting the effective progress of the photocatalytic reaction. Additionally, it confirms that the spillage of PDMS resin, resulting from mutual extrusion, securely loads the surface catalyst material. The 3D rendering provides a depiction of the substrate's transparent middle layer and the layer containing the active layer.

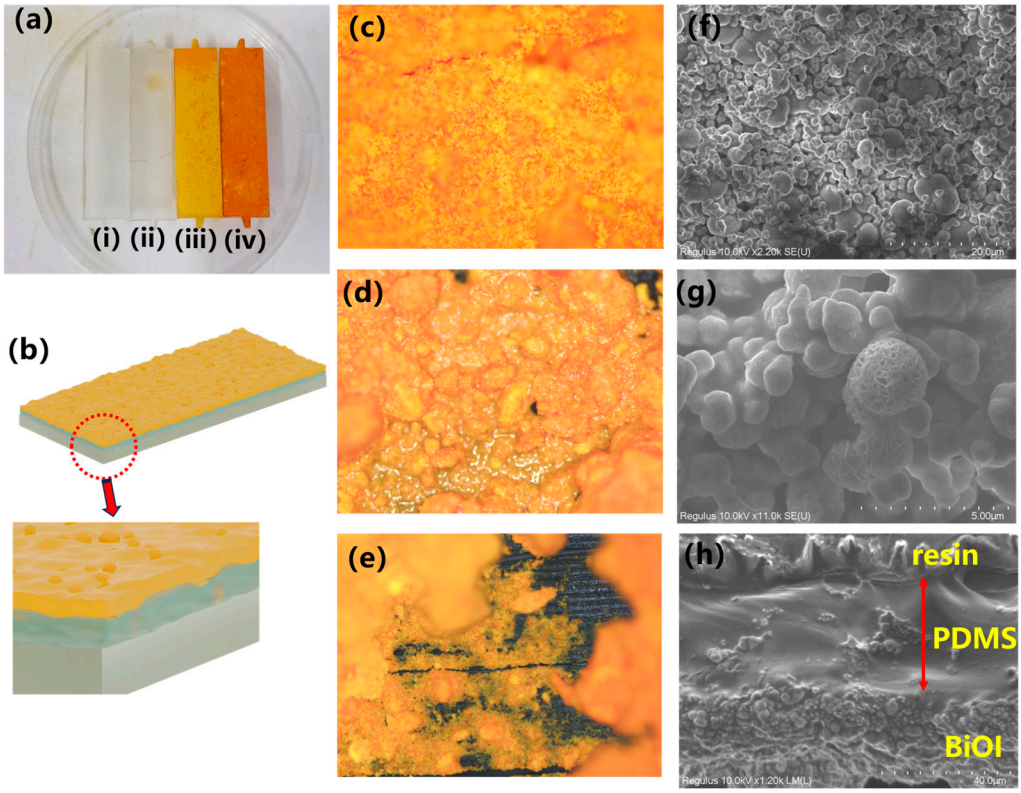

Figure 1. (**a**) The condition of the substrate's surface at various preparation stages, (**b**) 3D modeling illustrating the effect of the photocatalytic active layer, (**c**–**e**) images captured using a metallographic microscope, and SEM images of the surface (**f**,**g**) and cross section (**h**).

The light absorption capacity of pure BiOI and BiOI loaded on a substrate prepared using 3D printing technology was analyzed using UV-vis DRS (Hitachi U4100 UV–vis spectrometer, Hitachi, Ibaraki, Japan) and is depicted in Figure 3. The transparent substrate shows a relatively stable absorption intensity in the ultraviolet and visible light absorption regions. Both pure BiOI and BiOI loaded on the substrate display a similar trend in curve variation, with the light absorption edge occurring around 600 nm. Thus, the loaded material has a significant impact on the light absorption performance of the active layer substrate depending on the wavelength. Additionally, the figure illustrates a slight increase in the absorption strength after loading BiOI onto the substrate. This increase can be attributed to the transparent properties of the polypropylene resin used in the substrate and the PDMS resin used in the bonding layer.

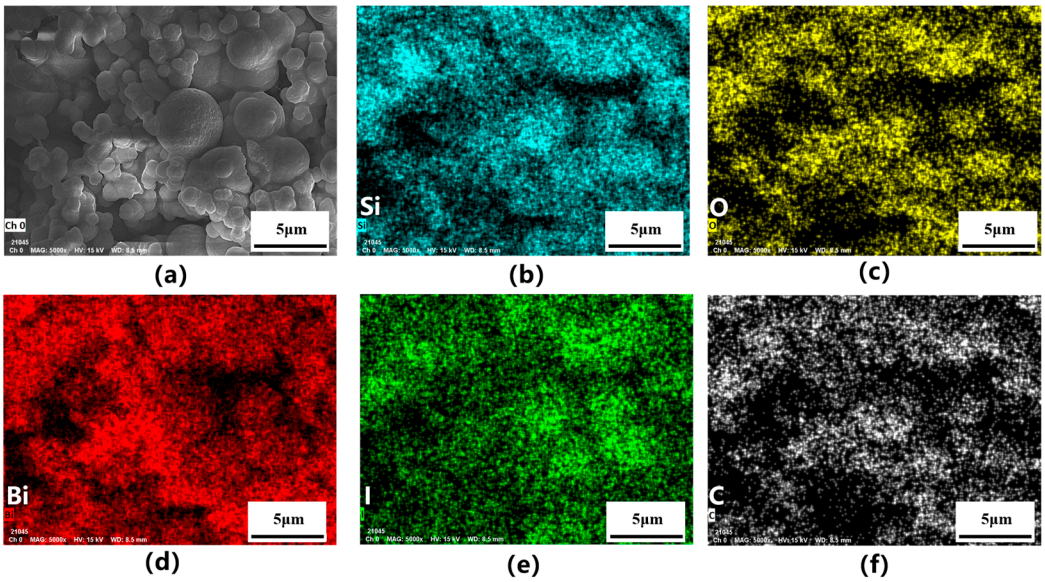

Figure 2. The surface of the active layer's SEM image (**a**) and its corresponding elemental mappings of (**b**) Si, (**c**) O, (**d**) Bi, (**e**) I and (**f**) C.

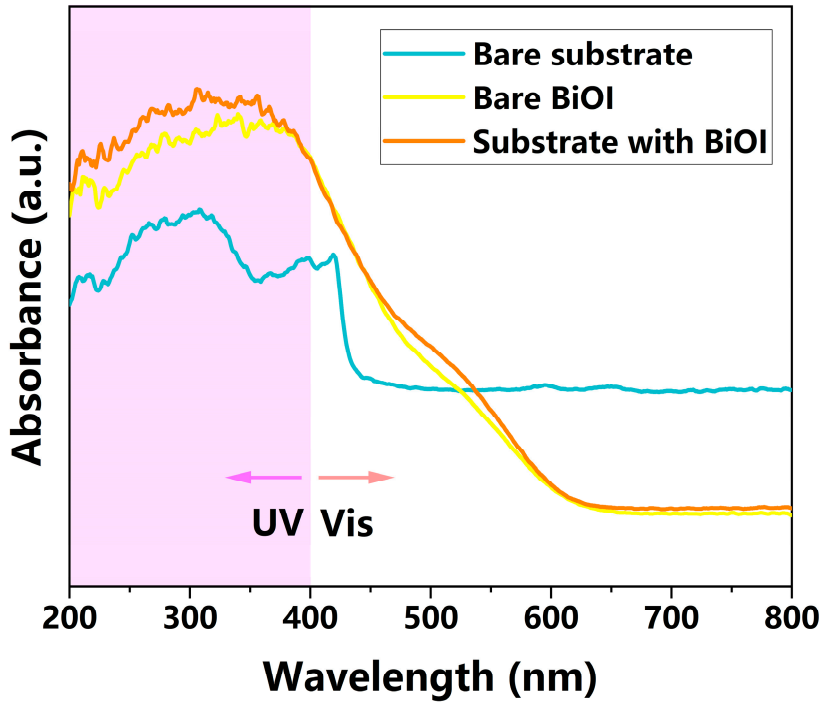

Figure 3. UV–vis DRS spectra of different part.

2.2. An Evaluation of the Photocatalytic Performance of the Water Purification Reactor Device

The reactor components fabricated using 3D printing technology provide advantages in terms of mass production and ease of replacement in case of damage, as they can be readily retrieved from water. Furthermore, the self-selecting power lamp source used in this study facilitates the rapid occurrence of photocatalytic reactions, distinguishing it from many other reactors constructed. To assess the photocatalytic water purification capability of the reactor in a sewage environment, typical model dyes (Rh B and MB) and model bacteria (*E. coli* and *S. aureus*) were chosen for this study.

In the experiment to evaluate the degradation of organic dyes, the reactor was initially immersed in a solution with a dye concentration of 10 mg/L and a solution volume of

60 mL. After a 30 min period of darkness to establish adsorption–desorption equilibrium, the reactor was irradiated using a 12 W LED for 2 h. Throughout the process, the samples were periodically extracted for testing and observation, as shown in the figure. Figure 4 illustrates the outstanding photocatalytic activity of the constructed reactor, achieving a degradation efficiency of 99.66% for Rh B and 88.10% for MB. Meanwhile, the figure also shows the degradation rate in the reaction tank when the reactor skeleton is not loaded with catalysts, and the results show that the pure photolysis reaction without the introduction of a photocatalyst has no obvious effect on the concentration of dye. An analysis of the curves indicates an initially rapid degradation rate for both dyes, followed by a gradual decrease. These experimental findings emphasize the effectiveness of the photocatalytic active layer fabricated using the mechanical extrusion method, which demonstrates excellent degradation performance against a broad range of macromolecular dyes.

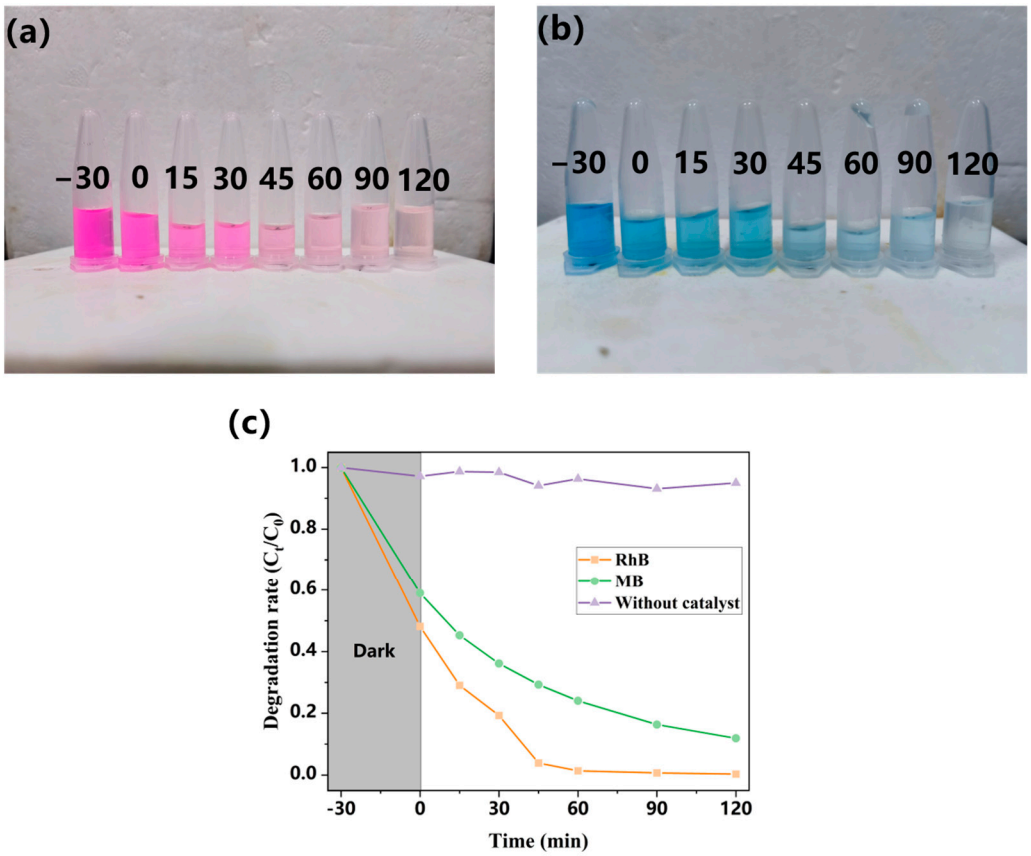

Figure 4. Solution color at different sampling times for (**a**) Rh B and (**b**) MB. (**c**) Degradation dynamics of Rh B, MB, and reactor skeleton without loading with catalysts.

Extensive research has focused on the photocatalytic eradication effect of BiOI on Gram-negative *E. coli* and Gram-positive *S. aureus*. However, additional research is required to investigate the photocatalytic bactericidal effect of the reactor constructed using this material. After a 2 h irradiation period, both *E. coli* and *S. aureus*, initially present at colony concentrations of 8.8 × 105 CFU/mL and 9.37 × 105 CFU/mL, respectively, exhibited a bactericidal effect of 99.99% (Figure 5a,c). The use of model dyes or model bacteria to simulate real sewage environments is crucial for guiding the practical application of photocatalytic reactors. However, evaluating the water purification capabilities of the constructed photocatalytic reactor in real water environments and assessing its effectiveness over time is crucial. Water samples collected from a natural lake underwent photocatalytic treatment to meet the drinking water standard of a colony count below 100 CFU/mL. In this study, water samples from the lake were regularly collected and cultured in beef paste medium during photocatalytic sterilization. As shown in Figure 5b,d, the initial bacterial

concentration in the collected water sample was approximately 3.7356 log10 CFU/mL. After 4 h of light exposure, the bacterial concentration decreased to 1.8129 log10 CFU/mL, meeting the international drinking water quality standards. In comparison to the bactericidal effect observed in simulated water environments, the reactor demonstrated a slower microbial kill rate in real water samples, possibly due to the higher complexity of microbial species and communities present in actual water environments.

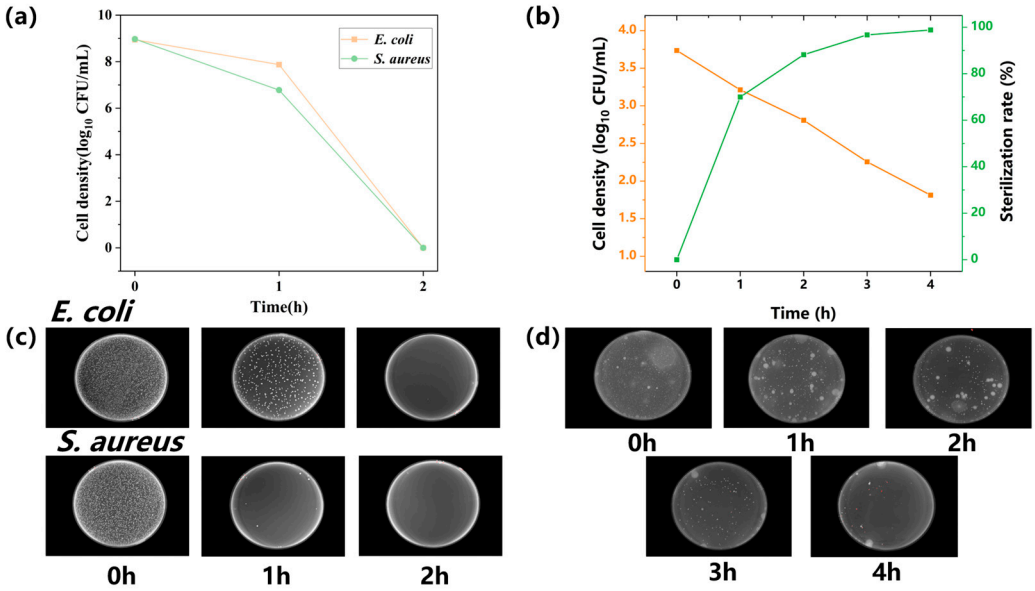

Figure 5. Photocatalytic sterilization in reactor. (**a**,**c**) *E. coli* and *S. aureus*; (**b**,**d**) actual water sample).

2.3. Load Stability of Photocatalytic Water Purification Reactor

The majority of reported photocatalytic reactors primarily emphasize high catalytic activity, overlooking the significance of load stability. However, it is essential to construct reactors capable of withstanding the demands of real-world working environments. Utilizing 3D printing to fabricate specific reactor components can enhance the anti-aging properties and chemical stability of polypropylene resin, ensuring its long-lasting performance in water. Furthermore, incorporating a jack-type connection between accessories enables the swift replacement of damaged parts.

2.3.1. The Recycling Stability of the Reactor

The Rh B dye was used as a standard for cyclic photocatalytic degradation to assess the recycling stability of the reactor. Each cycle consisted of a 0.5 h dark condition followed by a 2 h light condition. After each cycle, the solution inside the reactor was replaced with a solution of the same concentration and volume, and the cycle was restarted. The degradation activity, as shown in Figure 6, remained consistently within the range of 92.50 ± 4% after 50 cycles without any noticeable downward trend. A degradation curve was generated to represent the degradation process at the 0th, 10th, 20th, 30th, 40th, and 50th cycles. The degradation rate consistently exhibited similarity throughout, indicating the stable loading of the photocatalytic active layer onto the polypropylene resin substrate via mechanical extrusion.

The substrate was observed under an SEM after 50 cycles. The SEM images showed no significant detachment of the photocatalytic active layer compared to the images obtained before cyclic degradation (Figure 6c). This observation further suggests that the active sites were not covered even after 50 cycles of degradation testing, affirming the sustained high catalytic activity of the reactor.

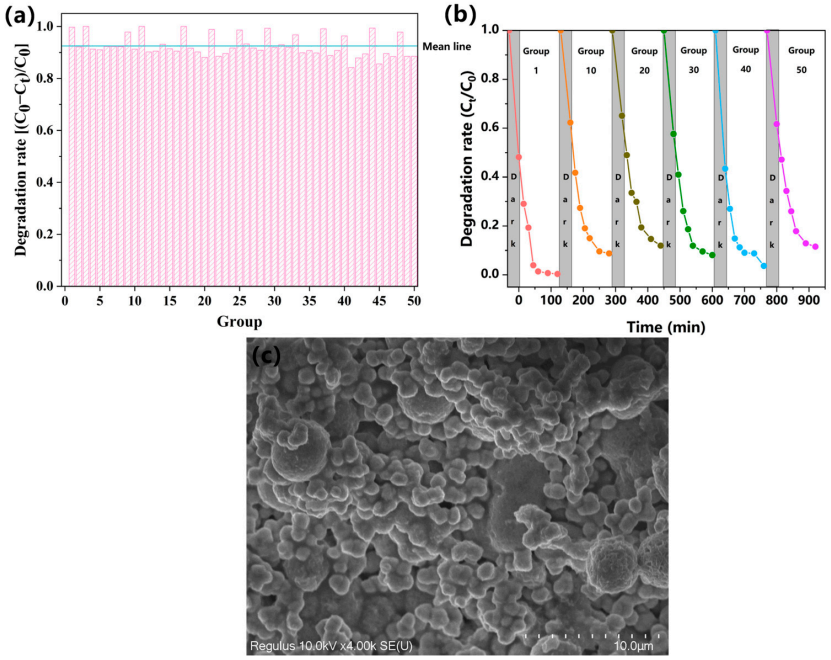

Figure 6. (**a**) Degradation of Rh B through 50 cycles. (**b**) Degradation dynamics at multiples of 10 in cycle. (**c**) SEM image after 50 cycles.

2.3.2. Simulated Scour Stability of Reactor

To evaluate the suitability of the interfacial binding force and resistance to water flow scouring in the photocatalytic water purification reactor, an experiment was conducted. The reactor was submerged in a beaker filled with 3 L of water and stirred at 1000 rpm for 24 h to simulate limiting water scouring. The resulting figure shows the condition of the active layer after scouring (Figure 7). Importantly, no significant detachment of the active layer was observed on the substrate surface following exposure to high-speed water flow for 24 h. Additionally, a comparison of the photocatalytic activity and rate constant of Rh B degradation in the reactor before and after scouring demonstrated the effective and relatively stable loading of BiOI onto the substrate surface under the influence of PDMS resin.

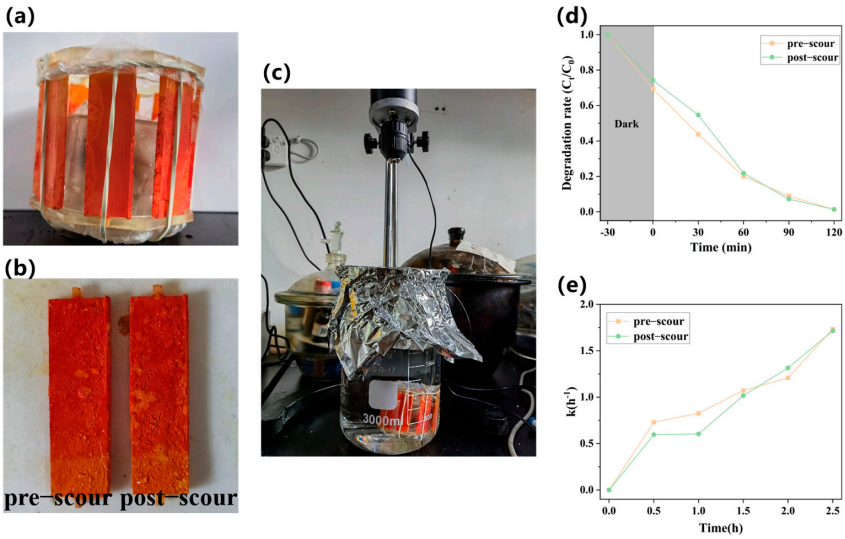

Figure 7. (**a**) The improved reactor skeleton. (**b**) An optical image of the reactor skeleton pre-scour and post-scour. (**c**) A physical diagram of the simulated scour experiment. (**d**) The degradation rate of Rh B before and after scouring. (**e**) The degradation dynamics of Rh B before and after scouring.

3. Materials and Methods

3.1. Chemicals and Materials

All chemicals and reagents used in this study for experimental applications were of analytical grade and deemed suitable for use without further purification, adhering to established standards. Bismuth nitrate pentahydrate ($Bi(NO_3)_3 \cdot 5H_2O$), potassium iodide (KI), and ethylene glycol (EG) were specifically obtained from Sinopharm Chemical Reagent Co., Ltd. The 3D printing resin and PDMS employed in the 3D printer were procured from Taobao.

3.2. Synthesis of BiOI

Amounts of 4 mmol of $Bi(NO_3)_3 \cdot 5H_2O$ and 4 mmol of KI were dissolved separately in 30 mL and 10 mL of EG, respectively. Each solution was stirred using a magnetic stirrer for 1 h. The resulting solutions, referred to as solution A and solution B, were obtained. Solution A was then slowly added to solution B with continuous stirring for 2 h. The resulting mixture was transferred to a Teflon reactor and allowed to react at a temperature of 413 K for 1 h. Subsequently, the mixture was centrifuged, and the resulting precipitate was washed three times with deionized water and anhydrous ethanol. Finally, the precipitate was dried in an oven at a temperature of 333 K for 12 h [48].

3.3. The Preparation and Characterization of the Photocatalytic Active Layer

To prepare the highly efficient and durable photocatalytic active layer of BiOI, the following steps were performed (Figure 8): In Step 1, the BiOI powder was finely ground to ensure the absence of large particles. In Step 2, the powder was evenly distributed by carefully pouring it into a 3D-printed square flute container specifically designed for this purpose. In Step 3, on one side of the 3D-printed cuboid polymer substrate made of polyacrylic polymer (PP), a PDMS resin was applied in a 10:1 ratio. In Step 4, a small amount of BiOI powder was transferred into a centrifuge tube, followed by the placement of the PP base with the PDMS layer inside the tube. The mixture was briefly shaken before removing the base from the tube. In Step 5, the base was then positioned in the groove, covered, and subjected to mechanical extrusion for a duration of 3 min. This entire process is illustrated in the figure provided below. The square groove prototype in the self-designed 3D printing device was inspired by the glass groove used in the XRD test. The cuboid shape of the base promotes the formation of a stable photocatalytic active layer through mechanical extrusion and is also utilized in the construction of the subsequent reactor. The measurements, carried out using scanning electron microscopy (SEM, Regulus 8100), a metallographic microscope (OLYMPUS BX53M, Olympus, Tokyo, Japan), and UV–vis diffuse reflectance absorption (UV–vis DRS, Hitachi U4100 UV–vis spectrometer), are used in this study.

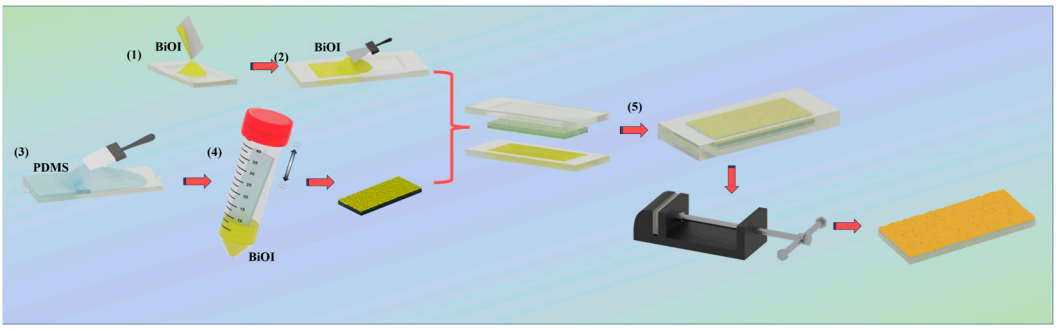

Figure 8. The procedure for the fabrication of a photocatalytic active layer on a 3D-printed substrate made of polyacrylic resin.

3.4. The Design of the Photocatalytic Reactor Based on the "Kongming Lantern" Standard

In this study, we present a novel design for a photocatalytic reactor device, drawing inspiration from the traditional Chinese "Kongming lantern" (Figure 9). The device is composed of two main components: the "lamp shade" and the "wick", which function as the carrier for the photocatalytic material and the light source, respectively. The "lamp shade" consists of two octagonal bases and eight individual "lamp surfaces", each equipped with a photocatalytic active layer. For the light source, the appropriate "wick" can be chosen depending on the desired LED power. In our specific research, we utilized a 12 W LED light source combined with BiOI to conduct a series of subsequent experimental investigations. In this reactor, the LED light is 5 mm away from the photocatalytic active layer, and its maximum light intensity is 163.7 W/m^2. Under this light intensity, the utilization rate of the active layer can reach 77.78%. When a photocatalytic reaction is performed, the reactor is placed in a square container filled with ice water to further eliminate the heat emitted during the reaction [49].

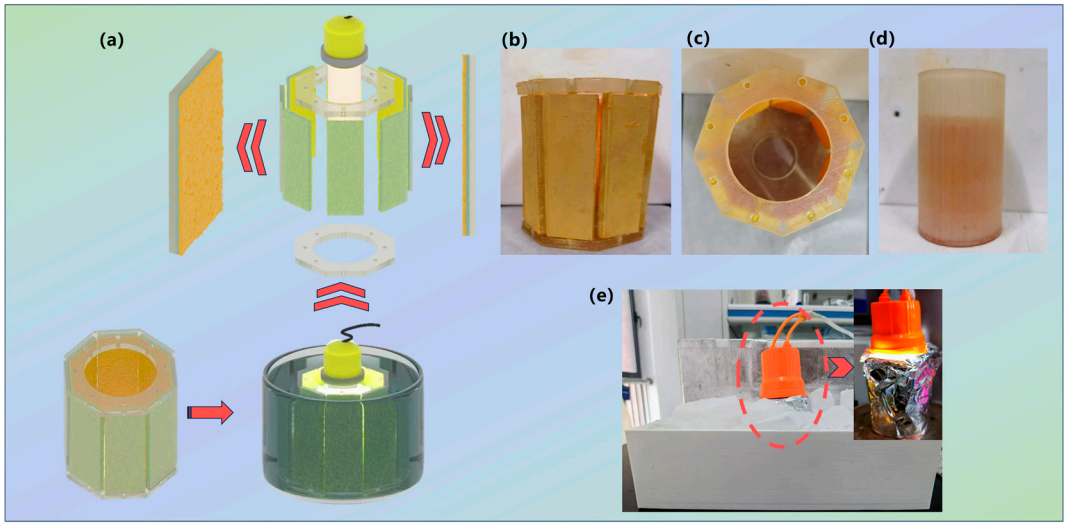

Figure 9. Various perspectives of the photocatalytic reactor: (**a**) the assembly process, (**b**) the front view of the reactor, (**c**) the top view of the reactor, (**d**) the front view of the complete device, and (**e**) the reactor during the photocatalytic reaction.

3.5. Evaluation of Photocatalytic Activity

The photocatalytic activity of the water purification reactor was investigated using two methods: the degradation of colored organic dyes and microbial killing tests. To conduct a comprehensive assessment of its effectiveness, a custom cylindrical container with specific dimensions (Φ = 50 mm; h = 100 mm) was 3D-printed to simulate a contaminated water environment. In the following test experiments, the solutions were prepared in advance and added to the reaction tank before the reaction began, while these solutions were prepared directly without any intervention in their temperature and pH value. For example, Rhodamine B solution for photocatalytic degradation experiments was always kept at room temperature with pH = 6.9 $\pm$ 0.1.

3.5.1. Photocatalytic Degradation of Different Colored Organic Dyes

For the sake of evaluating the photocatalytic degradation activity of macromolecular organic dyes commonly found in polluted water, Rh B and MB were selected as representative dyes for testing purposes. In addition, the reactor that was not loaded with a photocatalyst was placed directly in the reaction tank to check the pure photolysis reaction.

In order to adapt to the capacity of the reaction pool and better evaluate the degradation capacity of the reactor, 60 mL of Rh B or MB solution with a concentration of 10 mg/L was added to the reaction tank [50]. After the reactor device and 12 W LED light

source were placed in the reaction pool, the reactor was darkened for 30 min, and then the light source was turned on for 2 h. Specific experimental procedures can be found in the Supplementary Materials Text S1.

3.5.2. Bactericidal Activity against Conventional Gram-Negative and Gram-Positive Bacteria

Utilizing insights from previous laboratory research, the Gram-negative bacteria *E. coli* and the Gram-positive bacteria *S. aureus* were chosen as model organisms to assess the reactor's efficacy in eliminating microorganisms within polluted water. To replicate real-world conditions, bacterial concentrations comparable to those found in domestic polluted water, i.e., 10^5 CFU/mL, were employed. Taking the capacity of the reaction tank into account, 60 mL of "standardized cell suspension" was added to the reaction tank, and then the constructed reactor and 12 W LED light source were also put into it. Specific experimental procedures can be found in the Supplementary Materials Text S2.

3.5.3. Photocatalytic Microbial Killing Activity in Environmental Water Samples

To thoroughly evaluate the reactor's water purification capabilities within a genuine water environment, water samples were extracted from a lake in Qingdao, China (36.07° N, 120.35° E). Due to the wide variety of bacteria in the water and different requirements for nutrition and other growth conditions, it is impossible to find a medium under one condition to make all bacteria in the water grow and reproduce, so an ordinary beef extract peptone AGAR medium plate is usually used to grow out of the bacterial colony, from which it can calculate the total number of bacteria in the water as an approximation. After simple filtration of the obtained environmental water sample, 60 mL of the sample is added to the reaction pool, and the reactor device and 12 W LED light source are also put into it while adhering to industry standards (Water quality—Determination of total bacteria—Plate count method, HJ 1000-2018, published by the Ministry of Ecology and Environment of China in 26 December 2018) for measuring the reactor's water purification efficiency. The effect of water purification shall refer to the national sanitary standard for drinking water (Standards for drinking water quality, GB 5749-2022, published by the Standardization Administration of China in 15 March 2022) [51]. Specific experimental procedures can be found in the Supplementary Materials Text S3.

3.6. Stability Test of Photocatalytic Active Layer Loading

3.6.1. Cyclic Stability Test of Reactor's Photocatalytic Activity

For the sake of assessing the practical applicability of the reactor, it is crucial to evaluate its reusability and stability. Building upon the results of previous photocatalytic performance tests, we conducted a cyclic stability test using Rh B. The test involved alternating periods of 0.5 h in a dark state and 2 h under light conditions. The concentration and volume used were the same as those described in Section 3.5.1.

3.6.2. Stability Test of Material Loading in Simulated Oceanic Current Erosion Environment

Considering the potential application scenarios of the photocatalytic reactor, including both freshwater and seawater environments, the stability of the reactor's loaded materials in the presence of water flow erosion becomes a critical aspect to examine. To simulate these conditions, we subjected the photocatalytic reactor to extreme/current oceanic currents with high-speed agitation using a mixer. Additionally, with the assistance of 3D printing, we scaled up certain components of the original device to better evaluate their performance.

4. Conclusions

To achieve a more stable photocatalyst load on the substrate and optimize the balance between catalytic activity and reactor lifespan, a PDMS bond layer was applied to the surface of the 3D-printed substrate. Interaction forces were generated through mechan-

ical extrusion to ensure the stable loading of the active layer onto the bond layer. The construction of the photocatalytic reactor included the use of polyacrylic resin accessories known for their transparency, stable mechanical properties, and chemical stability. This approach allowed for customizable LED power to meet specific usage needs and prompt replacement based on the active layer's service life. The reactor exhibited outstanding photocatalytic performance with a degradation rate of 99.66% for Rh B and 88.10% for MB. It effectively eliminated *E. coli* and *S. aureus*, achieving a kill rate exceeding 99.99% within 2 h. Furthermore, the reactor demonstrated significant water purification capabilities for real water samples, meeting international drinking water quality standards within 4 h. Notably, the developed photocatalytic reactor unit combines high catalytic activity with long-term durability, surpassing existing units. Even after 50 weeks of cyclic degradation, an average degradation rate of 92.50% was consistently maintained, demonstrating sustained performance. This proposed photocatalytic reactor offers new insights and solutions for advancing green water purification technologies in line with "double carbon" goals. Additionally, it establishes a new benchmark for the loading method of photocatalytic materials and the optimization of reactor configuration.

Supplementary Materials: The following supporting information can be downloaded at https://www.mdpi.com/article/10.3390/catal14090645/s1, Text S1. Photocatalytic degradation of different colored organic dyes; Text S2. Bactericidal activity against conventional Gram-negative and Gram-positive bacteria; Text S3. Photocatalytic microbial killing activity in environmental water samples.

Author Contributions: Conceptualization, X.X. and Y.W.; methodology, X.X., Y.W. and J.W.; formal analysis, X.X.; investigation, X.X.; data curation, X.X.; writing—original draft preparation, X.X.; resources, Y.W., P.W. and D.Z.; writing—review and editing, Y.W.; supervision, Y.W. and D.Z.; funding acquisition, Y.W., J.W., P.W. and D.Z.; software, Z.D. and X.W. All authors have read and agreed to the published version of the manuscript.

Funding: This research was funded by the National Natural Science Foundation of China (Grant No. 42176047 and No. 42306227), the Postdoctoral Fellowship Program of CPSF (funded by China Postdoctoral Science Foundation, Grant No. GZB20230768), the 73rd batch of general support from the China Postdoctoral Science Foundation (funded by China Postdoctoral Science Foundation), the 2022 Special Research Assistant Program of the Chinese Academy of Science (funded by Chinese Academy of Sciences), and the Second Batch of Postdoctoral Funding in Qingdao in 2022 (funded by Qingdao City).

Data Availability Statement: The original contributions presented in this study are included in this article; further inquiries can be directed to the corresponding authors.

Conflicts of Interest: The authors declare no conflicts of interest.

References

1. Cao, Y.; Kong, L.; Ouyang, Z. Characteristics and Driving Mechanism of Regional Ecosystem Assets Change in the Process of Rapid Urbanization—A Case Study of the Beijing–Tianjin–Hebei Urban Agglomeration. *Remote Sens.* **2022**, *14*, 5747. [CrossRef]
2. Zhang, L.; Gu, Q.; Li, C.; Huang, Y. Characteristics and Spatial–Temporal Differences of Urban "Production, Living and Ecological" Environmental Quality in China. *Int. J. Environ. Res. Public Health* **2022**, *19*, 15320. [CrossRef] [PubMed]
3. Cheng, J.; Yu, B.; Zheng, R.; Wang, X.; Liu, J.; Wu, X.; Qin, L. Applications of Advanced Oxidation Technologies for Sludge Treatment. *IOP Conf. Series Earth Environ. Sci.* **2019**, *252*, 042044. [CrossRef]
4. Kadam, R.; Khanthong, K.; Park, B.; Jun, H.; Park, J. Realizable wastewater treatment process for carbon neutrality and energy sustainability: A review. *J. Environ. Manag.* **2023**, *328*, 116927. [CrossRef] [PubMed]
5. Li, D.; Wang, Z.; Yang, Y.; Liu, H.; Fang, S.; Liu, S. Research Status and Development Trend of Wastewater Treatment Technology and Its Low Carbonization. *Appl. Sci.* **2023**, *13*, 1400. [CrossRef]
6. Hodges, B.C.; Cates, E.L.; Kim, J.-H. Challenges and prospects of advanced oxidation water treatment processes using catalytic nanomaterials. *Nat. Nanotechnol.* **2018**, *13*, 642–650. [CrossRef]
7. Schneider, J.; Matsuoka, M.; Takeuchi, M.; Zhang, J.; Horiuchi, Y.; Anpo, M.; Bahnemann, D.W. Understanding TiO_2 Photocatalysis: Mechanisms and Materials. *Chem. Rev.* **2014**, *114*, 9919–9986. [CrossRef]
8. Prakash, M.; Kavitha, H.P.; Abinaya, S.; Vennila, J.P.; Lohita, D. Green synthesis of bismuth based nanoparticles and its applications—A review. *Sustain. Chem. Pharm.* **2022**, *25*, 100547. [CrossRef]

9. Ke, S.; Min, X.; Liu, Y.; Mi, R.; Wu, X.; Huang, Z.; Fang, M. Tungsten-Based Nanocatalysts: Research Progress and Future Prospects. *Molecules* **2022**, *27*, 4751. [CrossRef]
10. Wang, L.; Tong, Y.; Feng, J.; Hou, J.; Li, J.; Hou, X.; Liang, J. G-C3N4-based films: A rising star for photoelectrochemical water splitting. *Sustain. Mater. Technol.* **2019**, *19*, e00089. [CrossRef]
11. Du, Y.; Ma, R.; Wang, L.; Qian, J.; Wang, Q. 2D/1D BiOI/g-C3N4 nanotubes heterostructure for photoelectrochemical overall water splitting. *Sci. Total. Environ.* **2022**, *838*, 156166. [CrossRef] [PubMed]
12. Liao, X.; Li, T.-T.; Ren, H.-T.; Zhang, X.; Shen, B.; Lin, J.-H.; Lou, C.-W. Construction of BiOI/TiO_2 flexible and hierarchical S-scheme heterojunction nanofibers membranes for visible-light-driven photocatalytic pollutants degradation. *Sci. Total. Environ.* **2022**, *806*, 150698. [CrossRef] [PubMed]
13. Liu, Y.; Zhang, A.; Zhang, Q.; Mei, Y.; Wang, C.; Wang, Y.; Xiang, J.; Su, S.; Zhang, X.; Tan, Z. Facile synthesis of ternary AgBr/BiOI/$Bi_2O_2CO_3$ heterostructures via BiOI self-sacrifice for efficient photocatalytic removal of gaseous mercury. *Sep. Purif. Technol.* **2022**, *299*, 121722. [CrossRef]
14. Tong, Y.; Zhou, P.; Liu, Y.; Wang, N.; Li, W.; Cheng, F.; Yang, B.; Liang, J.; Zhang, Y.; Lai, B. Strongly enhanced Fenton-like oxidation (Fe/peroxydisulfate) by BiOI under visible light irradiation: A novel and green strategy for Fe(III) reduction. *J. Hazard. Mater.* **2022**, *428*, 128202. [CrossRef] [PubMed]
15. Zhang, B.; Wang, D.; Jiao, S.; Xu, Z.; Liu, Y.; Zhao, C.; Pan, J.; Liu, D.; Liu, G.; Jiang, B.; et al. TiO_2-X mesoporous nanospheres/BiOI nanosheets S-scheme heterostructure for high efficiency, stable and unbiased photocatalytic hydrogen production. *Chem. Eng. J.* **2022**, *446*, 137138. [CrossRef]
16. Wang, Y.; Long, Y.; Zhang, D. Facile in Situ Growth of High Strong BiOI Network Films on Metal Wire Meshes with Photocatalytic Activity. *ACS Sustain. Chem. Eng.* **2017**, *5*, 2454–2462. [CrossRef]
17. Xu, X.; Wang, Y.; Zhang, D. A novel strategy of hydrothermal in-situ grown bismuth based film on epoxy resin as recyclable photocatalyst for photodegrading antibiotics and sterilizing microorganism. *Sep. Purif. Technol.* **2022**, *290*, 120842. [CrossRef]
18. Xu, X.; Wang, Y.; Zhang, D.; Wang, J.; Yang, Z. In situ growth of photocatalytic Ag-decorated β-Bi_2O_3/$Bi_2O_{2.7}$ heterostructure film on PVC polymer matrices with self-cleaning and antibacterial properties. *Chem. Eng. J.* **2022**, *429*, 131058. [CrossRef]
19. Wang, Y.; Long, Y.; Yang, Z.; Zhang, D. A novel ion-exchange strategy for the fabrication of high strong BiOI/BiOBr heterostructure film coated metal wire mesh with tunable visible-light-driven photocatalytic reactivity. *J. Hazard. Mater.* **2018**, *351*, 11–19. [CrossRef]
20. Liu, G.; Xia, H.; Zhang, W.; Song, L.; Chen, Q.; Niu, Y. Improvement mechanism of NO photocatalytic degradation performance of self-cleaning synergistic photocatalytic coating under high humidity. *J. Hazard. Mater.* **2021**, *418*, 126337. [CrossRef]
21. Valenzuela, L.; Iglesias, A.; Faraldos, M.; Bahamonde, A.; Rosal, R. Antimicrobial surfaces with self-cleaning properties functionalized by photocatalytic ZnO electrosprayed coatings. *J. Hazard. Mater.* **2019**, *369*, 665–673. [CrossRef] [PubMed]
22. Liu, Y.; Huang, J.; Feng, X.; Li, H. Thermal-Sprayed Photocatalytic Coatings for Biocidal Applications: A Review. *J. Therm. Spray Technol.* **2020**, *30*, 1–24. [CrossRef] [PubMed]
23. Liu, G.; Xia, H.; Niu, Y.; Zhao, X.; Zhang, G.; Song, L.; Chen, H. Fabrication of self-cleaning photocatalytic durable building coating based on WO_3-TNs/PDMS and NO degradation performance. *Chem. Eng. J.* **2021**, *409*, 128187. [CrossRef]
24. El-Mekkawi, D.M.; Abdelwahab, N.A.; Mohamed, W.A.; Taha, N.A.; Abdel-Mottaleb, M. Solar photocatalytic treatment of industrial wastewater utilizing recycled polymeric disposals as TiO_2 supports. *J. Clean. Prod.* **2020**, *249*, 119430. [CrossRef]
25. Kanth, N.; Xu, W.; Prasad, U.; Ravichandran, D.; Kannan, A.M.; Song, K. PMMA-TiO_2 Fibers for the Photocatalytic Degradation of Water Pollutants. *Nanomaterials* **2020**, *10*, 1279. [CrossRef]
26. Ramasundaram, S.; Seid, M.G.; Choe, J.W.; Kim, E.-J.; Chung, Y.C.; Cho, K.; Lee, C.; Hong, S.W. Highly reusable TiO_2 nanoparticle photocatalyst by direct immobilization on steel mesh via PVDF coating, electrospraying, and thermal fixation. *Chem. Eng. J.* **2016**, *306*, 344–351. [CrossRef]
27. Wang, J.-C.; Li, Y.; Li, H.; Cui, Z.-H.; Hou, Y.; Shi, W.; Jiang, K.; Qu, L.; Zhang, Y.-P. A novel synthesis of oleophylic Fe_2O_3/polystyrene fibers by γ-Ray irradiation for the enhanced photocatalysis of 4-chlorophenol and 4-nitrophenol degradation. *J. Hazard. Mater.* **2019**, *379*, 120806. [CrossRef]
28. Wang, W.; Yang, R.; Li, T.; Komarneni, S.; Liu, B. Advances in recyclable and superior photocatalytic fibers: Material, construction, application and future perspective. *Compos. Part B Eng.* **2021**, *205*, 108512. [CrossRef]
29. Yang, Y.; Wu, T.; Que, W. Fabrication of Nanoparticle/Polymer Composite Photocatalytic Membrane for Domestic Sewage In Situ Treatment. *Materials* **2022**, *15*, 2466. [CrossRef]
30. Yu, H.; Jiao, Z.; Hu, H.; Lu, G.; Ye, J.; Bi, Y. Fabrication of Ag_3PO_4–PAN composite nanofibers for photocatalytic applications. *CrystEngComm* **2013**, *15*, 4802–4805. [CrossRef]
31. Chen, R.; Li, L.; Zhu, X.; Wang, H.; Liao, Q.; Zhang, M.-X. Highly-durable optofluidic microreactor for photocatalytic water splitting. *Energy* **2015**, *83*, 797–804. [CrossRef]
32. Gomes, J.; Maniezo, B.; Alves, P.; Ferreira, P.; Martins, R.C. Immobilization of TiO2 onto a polymeric support for photocatalytic oxidation of a paraben's mixture. *J. Water Process. Eng.* **2022**, *46*, 102458. [CrossRef]
33. Zhang, Y.; Huang, X.; Yeom, J. A Floatable Piezo-Photocatalytic Platform Based on Semi-Embedded ZnO Nanowire Array for High-Performance Water Decontamination. *Nano-Micro Lett.* **2019**, *11*, 1–14. [CrossRef] [PubMed]
34. Yahya, N.; Aziz, F.; Jamaludin, N.; Mutalib, M.A.; Ismail, A.; Salleh, W.W.; Jaafar, J.; Yusof, N.; Ludin, N.A. A review of integrated photocatalyst adsorbents for wastewater treatment. *J. Environ. Chem. Eng.* **2018**, *6*, 7411–7425. [CrossRef]

35. Li, M.; Hu, Z.; Liu, D.; Liang, Y.; Liu, S.; Wang, B.; Niu, C.; Xu, D.; Li, J.; Han, B. Efficient antibacterial and microbial corrosion resistant photocatalytic coating: Enhancing performance with S-type heterojunction and Cu synergy. *Chem. Eng. J.* **2024**, *495*, 153519. [CrossRef]
36. Zhang, Y.; Xu, Y.; Simon-Masseron, A.; Lalevée, J. Radical photoinitiation with LEDs and applications in the 3D printing of composites. *Chem. Soc. Rev.* **2021**, *50*, 3824–3841. [CrossRef]
37. Son, S.; Jung, P.-H.; Park, J.; Chae, D.; Huh, D.; Byun, M.; Ju, S.; Lee, H. Customizable 3D-printed architecture with ZnO-based hierarchical structures for enhanced photocatalytic performance. *Nanoscale* **2018**, *10*, 21696–21702. [CrossRef]
38. Zheng, Q.; Aiello, A.; Choi, Y.S.; Tarr, K.; Shen, H.; Durkin, D.P.; Shuai, D. 3D printed photoreactor with immobilized graphitic carbon nitride: A sustainable platform for solar water purification. *J. Hazard. Mater.* **2020**, *399*, 123097. [CrossRef]
39. Zhou, R.; Han, R.; Bingham, M.; O'rourke, C.; Mills, A. 3D printed, plastic photocatalytic flow reactors for water purification. *Photochem. Photobiol. Sci.* **2022**, *21*, 1585–1600. [CrossRef]
40. Borrello, J.; Nasser, P.; Iatridis, J.C.; Costa, K.D. 3D printing a mechanically-tunable acrylate resin on a commercial DLP-SLA printer. *Addit. Manuf.* **2018**, *23*, 374–380. [CrossRef]
41. González-Henríquez, C.M.; Sarabia-Vallejos, M.A.; Rodriguez-Hernandez, J. Polymers for additive manufacturing and 4D-printing: Materials, methodologies, and biomedical applications. *Prog. Polym. Sci.* **2019**, *94*, 57–116. [CrossRef]
42. Sim, J.-H.; Lee, S.H.; Yang, J.-Y.; Lee, W.-C.; Mun, C.; Lee, S.; Park, S.-G.; Cho, Y.-R. Plasmonic hotspot engineering of Ag-coated polymer substrates with high reproducibility and photothermal stability. *Sens. Actuators B Chem.* **2022**, *354*, 131110. [CrossRef]
43. Wen, Y.-T.; Dai, N.-T.; Hsu, S.-H. Biodegradable water-based polyurethane scaffolds with a sequential release function for cell-free cartilage tissue engineering. *Acta Biomater.* **2019**, *88*, 301–313. [CrossRef] [PubMed]
44. Schreck, M.; Kleger, N.; Matter, F.; Kwon, J.; Tervoort, E.; Masania, K.; Studart, A.R.; Niederberger, M. 3D Printed Scaffolds for Monolithic Aerogel Photocatalysts with Complex Geometries. *Small* **2021**, *17*, 2104089. [CrossRef] [PubMed]
45. Xu, X.; Xu, X.; Wang, Y.; Zhang, D.; Chen, C.; Yang, Z. In-situ growth pH-adjusted iodine defects engineering BiOI film on 3D-printed polymer substrate for efficient organic pollutant and microorganism purification. *Sep. Purif. Technol.* **2023**, *318*, 123974. [CrossRef]
46. Latif, A.; Memon, A.M.; Gadhi, T.A.; Bhurt, I.A.; Channa, N.; Mahar, R.B.; Ali, I.; Chiadò, A.; Bonelli, B. Bi_2O_3 immobilized 3D structured clay filters for solar photocatalytic treatment of wastewater from batch to scaleup reactors. *Mater. Chem. Phys.* **2022**, *276*, 125297. [CrossRef]
47. Li, N.; Tong, K.; Yang, L.; Du, X. Review of 3D printing in photocatalytic substrates and catalysts. *Mater. Today Energy* **2022**, *29*, 101100. [CrossRef]
48. Qiu, H.; Zhang, R.; Yu, Y.; Shen, R.; Gao, H. BiOI-on-SiO_2 microspheres: A floating photocatalyst for degradation of diesel oil and dye wastewater. *Sci. Total. Environ.* **2020**, *706*, 136043. [CrossRef]
49. Kiss, J.; Kukovecz, Z.; Kónya, Z. Beyond Nanoparticles: The Role of Sub-nanosized Metal Species in Heterogeneous Catalysis. *Catal. Lett.* **2019**, *149*, 1441–1454. [CrossRef]
50. Shi, Y.; Zhao, Q.; Li, J.; Gao, G.; Zhi, J. Onion-liked carbon-embedded graphitic carbon nitride for enhanced photocatalytic hydrogen evolution and dye degradation. *Appl. Catal. B Environ.* **2022**, *308*, 121216. [CrossRef]
51. *GB 5749-2022*; Standards for Drinking Water Quality. State Administration for Market Regulation, National Standardization Administration: Beijing, China, 2022.